INSTITUTE OF PHYSICS PUBLISHING JOURNAL OF PHYSICS D: APPLIED PHYSICS
J. Phys. D: Appl. Phys. **34** (2001) 2573–2580 PII: S0022-3727(01)22079-8

Coupled diffusional/displacive transformations: addition of substitutional alloying elements

S A Mujahid[1] **and H K D H Bhadeshia**[2]

[1]Radiation Physics Division, PINSTECH, P O Nilore, Islamabad, Pakistan
[2]University of Cambridge, Department of Materials Science and Metallurgy, Pembroke Street, Cambridge CB2 3QZ, UK

Received 19 February 2001, in final form 3 July 2001
Published 21 August 2001
Online at stacks.iop.org/JPhysD/34/2573

Abstract
A published theory for 'coupled diffusional/displacive transformations' is extended to alloyed steels in order to examine the nonequilibrium growth of partially supersaturated ferrite plates as a function of the carbon concentration. The model utilises three interface response functions i.e. the diffusion-field velocity, the interface mobility and the Aziz solute trapping function to enable the estimation of the three unknown quantities: supersaturation, velocity and the composition of austenite at the interface. It is found that the theory correctly predicts the variation in the martensite-start temperature with carbon concentration, but fails to estimate the corresponding variations in the bainite-start temperatures, the reasons for which are not clear.

1. Introduction

Solid-state phase transformations in steels can involve both substitutional and interstitial atoms. It is conceivable that the former do not diffuse during transformation, whereas the much more mobile interstitial atoms are able to partition between the parent (austenite, γ) and product (ferrite, α) phases. Thus, the lattice change could be accomplished by displacive transformation as far as the substitutional solute and iron atoms are concerned. There would then be an invariant-plane strain shape change (with a large shear component) associated with the growth of a thin-plate shaped product. The extent to which the carbon atoms partition during the growth of ferrite plates by this mechanism can in principle be between equilibrium and full supersaturation (i.e. zero partitioning).

An attempt has recently been made to model such growth involving some partitioning of carbon [1, 2], the rest being trapped as the α/γ interface advances. Whilst it is appreciated that models like these are currently less than satisfactory in predicting experimental behaviour [3], they are the only ones capable of giving some idea of the growth rates involved during displacive transformations which occur above the martensite-start temperature. The coupled diffusional/displacive transformation (CDDT) model has already been extended further to deal with a variety of plain carbon steels [4]. The purpose of the present work is to apply the modified CDDT model to a number of alloyed steels and to compare the results with the experimental data of Steven and Haynes [5] in order to check whether the model can be applied to alloyed steels. It was intended at the outset of this work to compare some of the overall results of such modelling with alternative, tried and tested but less informative methods of calculating transformation characteristics. Throughout this paper, an approximation is made that the solid solution strengthening caused by the introduction of relatively small concentrations of substitutional solute can be neglected. The interface mobility function is therefore indentified with that used for plain carbon steels.

2. The response functions

There are many processes, including diffusion, which occur in series as the ferrite grows. Each of these dissipates a proportion of the free energy available for transformation. For a given process, the variation in interface velocity with dissipation defines a function which in recent years has been called an *interface response function*. The actual velocity of the interface depends on the simultaneous solution of all the interface response functions, a procedure which fixes the composition of the growing particle.

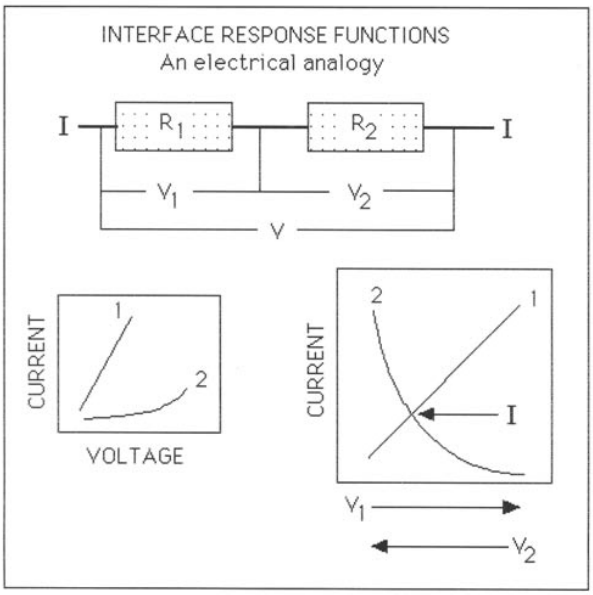

Figure 1. An electrical analogy illustrating the dissipations due to processes which occur in series as the transformation interface moves. The resistors in series are the hurdles to the motion of the interface, the voltage the driving force and the current the interface velocity. The way in which voltage (driving force) is dissipated as a function of current (velocity) across each resistor is different, since each resistor represents a separate physical process. There is only one interface so all these processes must yield the same velocity, as indicated by the identical current passing through all the resistors.

Figure 1 shows an electrical analogy; the resistors in series are the hurdles to the movement of the interface. They include diffusion in the parent phase, the transfer of atoms across the interface, solute drag etc. The electrical-potential drop across each resistor corresponds to the free energy dissipated in each process, and the current, which is the same through each resistor, represents the interface velocity. The relationship between the current and potential is different for each resistor, but the actual current is obtained by a simultaneous solution of all such relations.

Following on from this analogy, the available free energy can be partitioned into that dissipated in the diffusion of carbon, a quantity expended in the transfer of atoms across the interface, and in any other process determining the motion of the interface. There are three unknowns: the austenite composition at the interface, the supersaturation and the velocity, so it is necessary to exploit at least three interface response functions. If the tip radius of the plate is considered to be a variable, then the number of unknowns is four; for displacive transformations the radius can be assumed to be fixed by strain energy minimisation. The necessary three interface velocity functions are, therefore, the diffusion field velocity, the velocity determined from interface mobility and a carbon trapping function [1, 2].

These three processes (response functions) occur in series and the solution of each function must therefore give the same interfacial velocity. Their simultaneous solution can therefore be used to calculate the three unknown variables (temperature, interface velocity and supersaturation). These response functions are discussed briefly in this section. Further details are available in references [1, 2].

2.1. Diffusion-field velocity

The velocity during the steady state growth of ferrite plates may be approximated by the Ivantsov solution [6] for a parabolic cylinder, given by;

$$\frac{(\overline{x} - x_I)}{(x_\alpha - x_I)} = (\sqrt{\pi p}) \exp(p)\mathrm{erfc}(\sqrt{p})$$

where the Péclet number is

$$p = \frac{V_d \rho}{2\overline{D}}$$

and

$$\overline{D} = \int_{x_I}^{\overline{x}} \frac{D(x,T)dx}{(\overline{x} - x_I)}$$

is the weighted average diffusivity of carbon in austenite which is carbon concentration and temperature dependent [7, 8, 9]. ρ is the plate tip radius. $\overline{x}$, x_I and x_α are the average mole fraction of carbon in alloy, mole fraction of carbon in austenite at the γ/α interface and the mole fraction of carbon in ferrite at the α/γ interface respectively.

2.2. Interface mobility

The interface mobility of a moving α/γ boundary can be approximated by the theory of thermally activated dislocation motion [10, 11, 12];

$$V_i = V_0 \exp\left\{\frac{-Q^*}{kT}\right\}$$

where the free energy of activation

$$Q^* = Q_0\left\{1 - \left(\frac{G_{id}}{\hat{G}_{id}}\right)^y\right\}^z$$

and Q_0 is the total activation free energy to overcome the resistance to dislocation motion without the aid of interfacial driving force and has been calculated by using [13]. G_{id} is the Gibbs free energy per unit volume dissipated in the process of interfacial motion and $\hat{G}_{id}$ is the maximum glide resistance presented by obstacles to the dislocation motion. y and z are the constants which define the shape of the force-distance function [14] for solid-solution interactions, values of which were taken from [1, 2].

2.3. The solute trapping law

There is a large difference in the diffusivities of interstitial carbon and iron (or substitutional solutes). The possibility then arises that the substitutional lattice can be transformed by a displacive mechanism, while the carbon atoms redistribute between the parent and product phase [15]. The atoms which are forced into the product lattice, i.e. whose chemical potential is raised on transfer across the interface, are said to be *trapped* [16]. When it is the solute atoms whose chemical potential is raised on transfer across the interface, the phenomenon is called solute trapping.

The solute trapping velocity can be calculated by using the Aziz model [17, 18] of solute trapping during rapid solidification;

$$V_k = \frac{D\{x_I\}}{\lambda}\left(\frac{k_p - k_e}{1 - k_p}\right)$$

where partitioning coefficient

$$k_p = \frac{x_\alpha}{x_I}$$

and equilibrium partitioning coefficient

$$k_e = \frac{x^{\alpha\gamma}}{x^{\gamma\alpha}}.$$

λ is intersite distance taken to be 0.25 nm [2]. $x^{\alpha\gamma}$ and $x^{\gamma\alpha}$ are the equilibrium mole fractions of carbon in ferrite and in austenite respectively.

2.4. Solution of coupled equations

Each of the interface response functions provides a velocity as a function of the free energy dissipated in that particular process. The total driving force available has to be partitioned into the individual dissipations in such a way that all the response functions given an identical velocity. This is done in practice by numerically varying, on a computer model, the carbon supersaturation until this condition is satisfied. A graphical illustration of the procedure can be found in [19].

The parameters needed for the solution of the equations include the diffusion coefficient of carbon in austenite, as a function of its concentration. This is described in detail in [9]; this is available as a subroutine on MAP_STEEL_DIFFUS on the materials algorithms project [MAP] library on the world wide web [20]. All of the driving forces and equilibrium or partitioning coefficients were calculated using a quasichemical thermodynamic model described in [21] and available on MAP as a computer program MAP_STEEL_MUCG46.

3. Results and discussion

3.1. Martensite-start temperature

There are several methods for the prediction of martensite-start temperatures in steels, especially when the alloy concentration is small. The most commonly used method [5] is completely empirical and works rather well, with M_s being given, for example, by

$$M_s(^\circ C) = 561 - 474C - 33Mn - 17Ni - 17Cr - 21Mo \quad (1)$$

where the concentrations are all stated in weight percent. Using this relation, the M_s temperature can be calculated within $\pm$ 20–25°C with a 90% certainty within the following limits of chemical composition:

C $0.1 - 0.5$ wt% Cr Trace $- 3.5$ wt% Mn $0.2 - 1.7$ wt%

Mo Trace $- 1.0$ wt% Ni Trace $- 5$ wt%

A more general method which has its origins in the work by Kaufman and Cohen [22, 23] assumes that martensite forms at a temperature where the driving force for diffusionless transformation $\Delta G^{\gamma\alpha}$ reaches a critical value $\Delta G^{\gamma\alpha}_{M_s}$ (figure 2) Thus, alloying elements lead to a change in M_s simply as a consequence of their effect on the thermodynamic stabilities of the γ and α crystals.

Bhadeshia [24] used this method with experimental M_s data, to calculate $\Delta G^{\gamma\alpha}_{M_s}$ for a series of Fe–C alloys and found that external driving force is a function of the carbon concentration (figure 3). This function was then used empirically to predict the M_s temperatures for substitutionally alloyed steels [27], assuming that M_s is given by the temperature where $\Delta G^{\gamma\alpha}\{Fe{-}C{-}X, M_s\} = \Delta G^{\gamma\alpha}_{M_s}\{Fe{-}C\}$. The method works extremely well, but there is no justification for the particular way in which $G^{\gamma\alpha}_{M_s}\{Fe - C\}$ varies with the concentration of carbon.

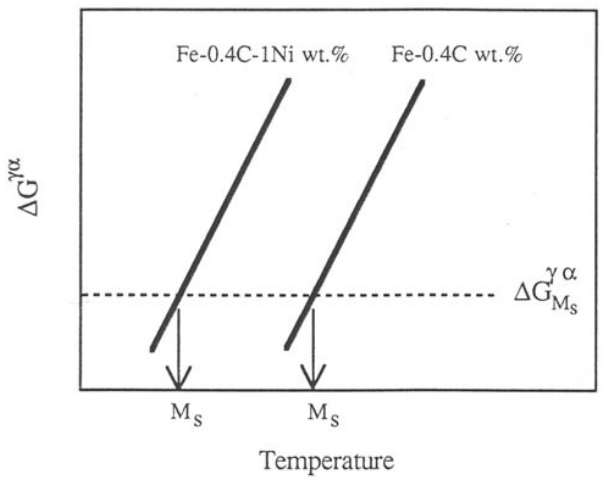

Figure 2. Schematic free energy curve illustrating the martensite formation at a critical value of free energy and the effect of alloying element.

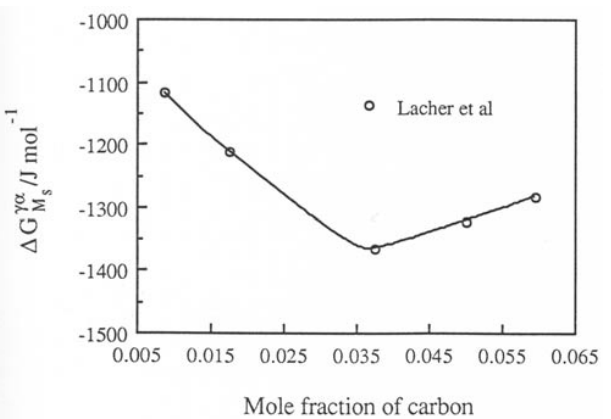

Figure 3. Variation of free energy change (accompanying martensitic transformation at M_s temperature) as a function of carbon content [24, 25, 26].

The CDDT method can in principle avoid all of the empirical assumptions discussed above. The experimental data of Steven and Haynes [5] provide a rich source of carefully measured M_s temperatures as a function of the alloy chemistry (Tables 1 and 2). The definition of the martensite-start temperature is that it corresponds to the temperature where both nucleation and growth become diffusionless. The CDDT model with the temperature dependent stored energy was applied to the Steven and Haynes data. The results are illustrated in figure 4; the level of agreement between the experimental data and those calculated is impressive and gives confidence in the CDDT model. During barrierless nucleation, the dependence of stored energy on M_s temperature is shown in figure 5. The variation in the driving force at M_s with M_s

Table 1. Chemical composition of steels analysed. The 'En' number used to be the common identification terminology incorporated in British Standards.

Reference No	B. S. En. No	Chemical Composition wt%								
		C	Si	Mn	S	P	Ni	Mo	Cr	V
1	12	0.34	0.20	1.06	0.040	0.037	0.75	0.02	0.08	–
2	12	0.33	0.21	0.62	0.025	0.022	0.89	0.05	0.10	–
3	13	0.19	0.14	1.37	0.012	0.026	0.56	0.31	0.20	–
4	14	0.29	0.26	1.67	0.030	0.033	0.21	0.04	0.12	–
5	15	0.33	0.23	1.54	0.024	0.021	0.18	0.05	0.15	–
6	16	0.33	0.18	1.48	0.028	0.028	0.26	0.27	0.16	–
7	17	0.38	0.25	1.49	0.028	0.036	–	0.41	–	–
8	18	0.39	0.16	0.89	0.025	0.027	0.25	Nil	0.88	–
9	18	0.48	0.25	0.86	0.021	0.023	0.18	0.04	0.98	–
10	19	0.41	0.31	0.64	0.017	0.030	0.18	0.38	1.24	–
11	19	0.41	0.23	0.67	0.016	0.015	0.20	0.23	1.01	–
12	21	0.33	0.23	0.74	0.027	0.031	3.47	–	0.07	–
13	22	0.40	0.26	0.62	0.005	0.007	3.45	0.10	0.28	–
14	23	0.33	0.23	0.57	0.007	0.005	3.26	0.09	0.85	–
15	23	0.32	0.28	0.61	0.031	0.018	3.22	0.22	0.63	0.03
16	24	0.36	0.22	0.52	0.005	0.007	1.52	0.27	1.17	–
17	24	0.38	0.20	0.67	0.010	0.017	1.58	0.26	0.95	–
18	25	0.32	0.27	0.56	0.012	0.018	2.37	0.51	0.74	–
19	25	0.31	0.20	0.62	0.012	0.018	2.63	0.58	0.64	–
20	26	0.38	0.15	0.56	0.005	0.011	2.42	0.46	0.74	–
21	26	0.42	0.31	0.67	0.022	0.029	2.53	0.48	0.72	–
22	28	0.32	0.19	0.51	0.009	0.013	3.02	0.48	1.37	0.18
23	28	0.25	0.15	0.52	0.024	0.010	3.33	0.65	1.14	0.16
24	30A	0.35	0.14	0.44	0.008	0.016	4.23	0.13	1.43	–
25	30B	0.33	0.17	0.51	0.009	0.013	4.16	0.31	0.44	–
26	30B	0.32	0.29	0.47	0.020	0.022	4.13	0.30	1.21	0.01
27	40B	0.26	0.21	0.55	0.022	0.010	0.25	0.54	3.34	–
28	45A	0.55	1.74	0.87	0.037	0.038	–	–	–	–
29	47	0.51	0.27	0.72	0.020	0.021	0.15	0.05	0.094	0.20
30	100	0.40	0.24	1.38	0.031	0.033	0.74	0.16	0.53	–
31	100	0.40	0.21	1.34	0.027	0.028	1.03	0.22	0.53	–
32	110	0.44	0.23	0.58	0.004	0.029	1.40	0.11	1.26	–
33	110	0.39	0.23	0.62	0.018	0.021	1.44	0.18	1.11	–
34	111	0.35	0.13	0.65	0.032	0.035	1.27	Nil	0.55	–
35	111	0.37	0.28	0.89	0.035	0.025	1.24	0.05	0.63	–
36	160	0.41	0.13	0.48	0.043	0.016	1.75	0.22	0.17	–
37	32A	0.14	0.19	0.50	0.043	0.031	0.19	0.06	0.16	–
38	33	0.10	0.25	0.46	0.006	0.007	3.00	0.12	0.13	–
39	34	0.25	0.16	0.40	0.021	0.019	1.78	0.27	0.23	–
40	35	0.24	0.17	0.42	0.005	0.010	1.84	0.20	0.18	–
41	36	0.14	0.19	0.46	0.009	0.006	3.55	0.12	1.11	–
42	36	0.15	0.25	0.41	0.008	0.020	3.02	0.15	0.90	–
43	37	0.09	0.33	0.33	0.031	0.018	4.87	0.08	0.13	–
44	38	0.11	0.21	0.30	0.004	0.014	5.04	0.30	0.13	–
45	39B	0.15	0.20	0.38	0.018	0.027	4.33	0.17	1.16	–
46	39B	0.14	0.28	0.45	0.017	0.016	4.11	0.24	1.11	–
47	39B	0.15	0.23	0.33	0.015	0.015	4.25	0.25	1.11	–
48	320	0.14	0.22	0.50	0.015	0.010	2.13	0.18	2.00	–
49	325	0.20	0.11	0.53	0.005	0.026	1.75	0.25	0.50	–
50	352	0.20	0.15	0.71	0.018	0.032	1.13	0.05	0.80	–
51	353	0.18	0.26	0.93	0.008	0.016	1.34	0.11	1.11	–
52	354	0.19	0.21	0.90	0.015	0.017	1.97	0.18	1.08	–
53	–	0.40	0.23	0.52	0.004	0.008	1.83	1.00	1.25	0.15
54	–	0.31	0.13	0.54	0.025	0.011	1.67	0.24	1.24	
55	–	0.41	0.35	0.58	0.020	0.013	1.43	0.31	1.27	–
56	–	0.49	0.17	0.52	0.022	0.013	1.50	0.29	1.28	–
57	–	0.38	0.33	0.55	0.021	0.010	0.16	0.31	1.25	–
58	–	0.38	0.12	0.56	0.024	0.017	3.00	0.29	1.21	–
59	–	0.38	0.12	0.57	0.023	0.010	4.95	0.29	1.22	–
60	–	0.41	0.15	0.52	0.027	0.016	1.46	0.29	2.10	–
61	–	0.37	0.12	0.52	0.026	0.012	1.51	0.29	2.90	–
62	–	0.40	0.30	0.55	0.025	0.011	1.47	0.52	1.22	–
63	–	0.36	0.16	0.56	0.029	0.009	1.46	0.31	1.22	0.13
64	–	0.39	0.26	0.20	0.022	0.009	1.66	0.26	1.22	–
65	–	0.40	0.27	0.84	0.025	0.012	1.75	0.27	1.23	–

Table 2. Comparison of predicted values of M_s and B_s with the experimental data [5] for a variety of alloys.

Reference No	B. S. En No	Experimental		Using CDDT model	
		M_s (° C)	B_s (° C)	M_s (° C)	B_s (° C)
1	12	345	–	365	420
2	12	370	–	385	520
3	13	420	600	410	535
4	14	380	560	361	427
5	15	340	–	350	–
6	6	340	580	350	418
7	17	320	550	335	398
8	18	320	560	345	396
9	18	300	560	310	356
10	19	320	540	335	397
11	19	330	570	335	402
12	21	310	570	330	386
13	22	280	540	303	401
14	23	300	500	323	380
15	23	320	520	325	387
16	24	325	530	339	400
17	24	320	530	335	381
18	25	335	510	340	402
19	25	330	500	335	349
20	26	305	520	315	373
21	26	290	480	295	349
22	28	315	440	305	366
23	28	330	470	325	392
24	30A	290	420	285	342
25	30B	295	420	285	343
26	30B	295	420	300	355
27	40B	360	450	347	411
28	45A	290	–	310	367
29	47	290	560	298	351
30	100	300	530	310	371
31	100	300	520	295	365
32	110	300	520	310	361
33	110	320	520	325	382
34	111	347	–	360	415
35	111	315	600	340	395
36	160	320	–	342	397
37	32A	–	–	–	–
38	33	–	–	–	–
39	34	–	–	–	–
40	35	–	640	–	542
41	36	415	550	385	362
42	36	415	580	402	534
43	37	–	–	–	–
44	38	390	550	395	452
45	39B	365	500	365	430
46	39B	390	500	375	435
47	39B	380	500	372	434
48	320	415	520	400	456
49	325	390	620	410	545
50	352	415	600	410	545
51	353	400	560	395	530
52	354	410	530	380	443
53	–	275	450	295	354
54	–	365	530	350	411
55	–	300	490	315	371
56	–	260	480	–	343
57	–	320	550	355	412
58	–	280	450	295	351
59	–	260	370	–	312
60	–	–	430	–	353
61	–	280	400	290	349
62	–	320	450	330	374
63	–	300	500	325	387
64	–	310	540	340	394
65	–	270	450	300	356

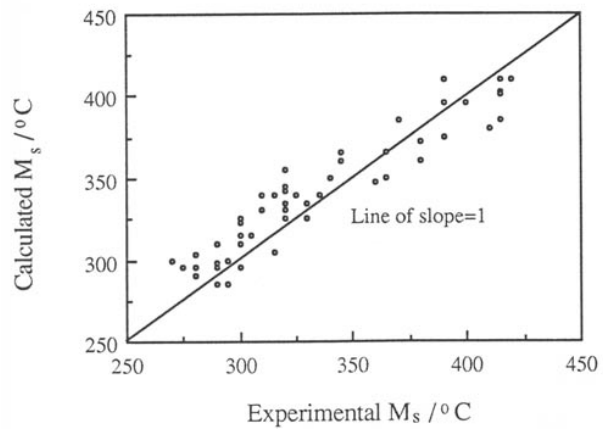

Figure 4. The agreement between the M_s as calculated using the CDDT model (with variable stored energy), and the experimental data of Steven and Haynes [5].

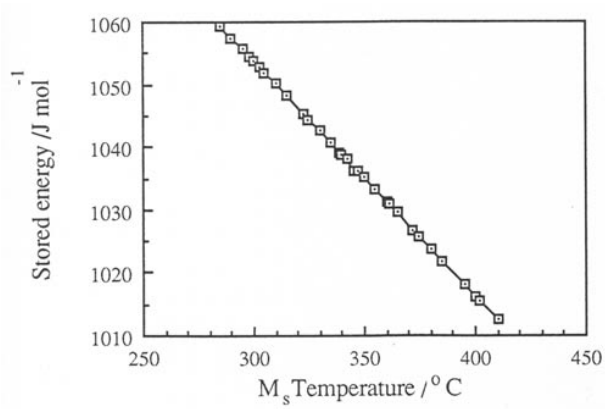

Figure 5. Variation of stored energy during nucleation at M_s versus M_s temperature of each alloy.

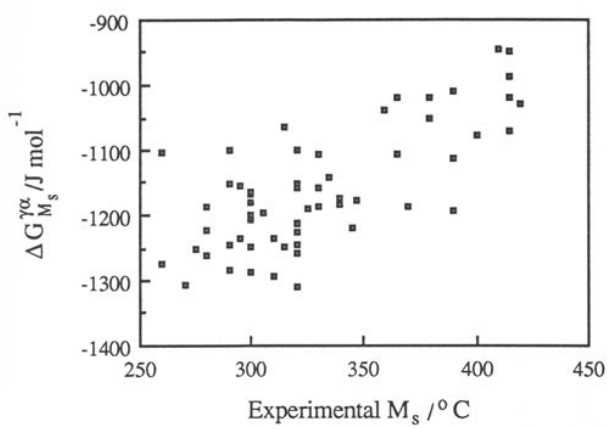

Figure 6. Plot of driving force at M_s versus M_s temperature of each alloy.

temperature is shown in figure 6. The predicted variation of $\Delta G^{\gamma\alpha}\{Fe-C, M_s\}$ with carbon concentration is compared against the Bhadeshia [24] results is shown in figure 7.

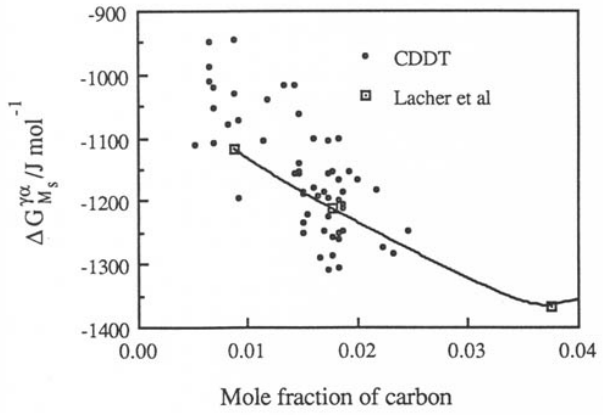

Figure 7. Comparison of the variation of free energy change (accompanying martensitic transformation at M_s temperature) as a function of carbon content between the predicted and the curve by Bhadeshia [24].

3.2. The bainite-start temperature

Again, for bainite, there are empirical equations for the variation in the B_s temperature with alloy chemistry [5];

$$B_s(^\circ C) = 830 - 270C - 90Mn - 37Ni - 70Cr - 83Mo \quad (2)$$

where the concentrations are all stated in weight percent. This relation calculates the B_s temperature within $\pm$ 20–25°C with a 90% certainty within the following limits of chemical composition:

C $0.1 - 0.5$ wt% Cr Trace $- 3.5$ wt% Mn $0.2 - 1.7$ wt%

Mo Trace $- 1.0$ wt% Ni Trace $- 5$ wt%

However, the precision with which such equations represent B_s is known to be poor when compared with corresponding equations for M_s temperature. Part of the reason for this is that the B_s temperature is much more difficult to measure. In some low-alloy steels, there is an overlap of several reactions in the vicinity of the bainite transformation temperature range, and this can confuse measurements. Secondly, as pointed out in a detailed analysis by Bhadeshia [28], some authors confuse the onset of Widmanstätten growth with that of bainite.

A more fundamental method for estimating B_s is given by Bhadeshia; it sets two conditions for the formation of bainite:

(a) That the driving force for diffusionless growth must exceed the stored energy of bainite ($\simeq$ 400 J mol^{-1})

$$\left|\Delta G^{\gamma\alpha}\right| > 400 \quad \text{J mol}^{-1}$$

(b) That the driving force for nucleation ΔG_m (during which carbon partitions between the parent phases) must exceed a value $G_N\{T\}$

$$\left|\Delta G_m\right| > \left|G_N\{T\}\right|$$

G_N is a universal function for displacive nucleation and is independent of alloy chemistry — it has been defined by Bhadeshia [28]. The method is illustrated in figure 8. When these two conditions are simultaneously satisfied, bainite transformation becomes feasible.

The method works quite well in predicting the B_s temperature. Although the function G_N is based on and

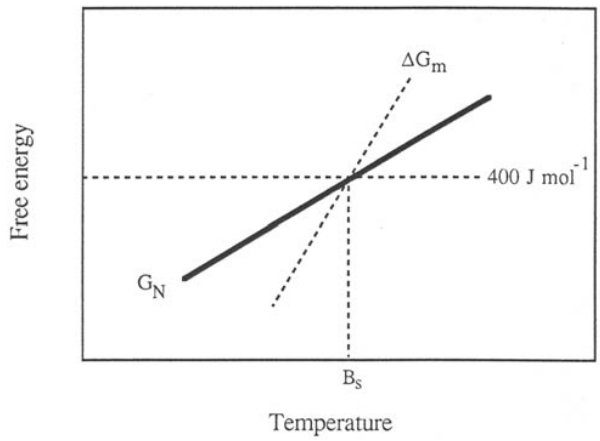

Figure 8. Schematic free energy versus temperature curve illustration showing the conditions of determining bainite start temperature.

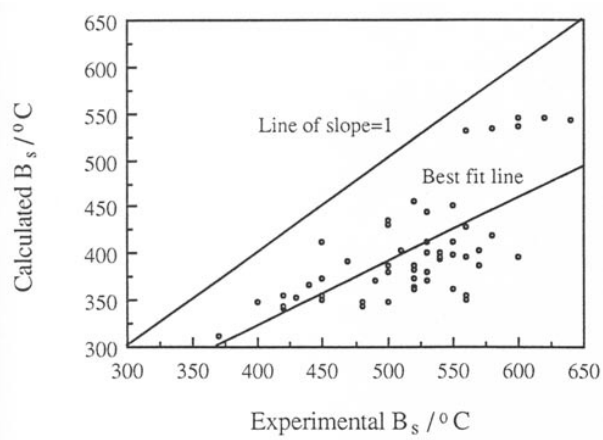

Figure 9. The B_s as calculated using the CDDT model (with variable stored energy) and assuming that bainite growth is diffusionless, versus the experimental data of Steven and Haynes [5].

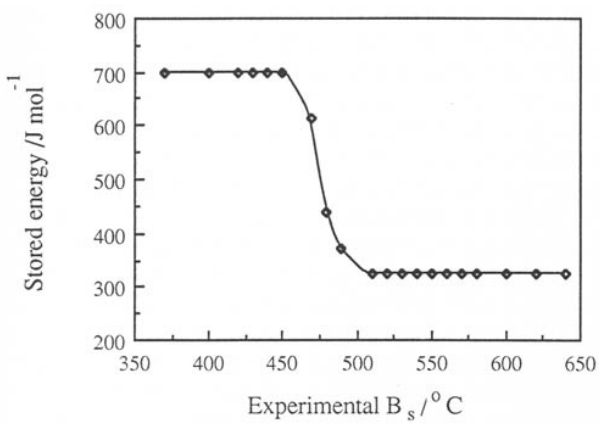

Figure 10. Plot of stored energy at experimental values of B_s [5] for each alloy.

consistent with the physical properties of displacive nucleation theory, there is a certain amount of fitting involved in deriving certain constants for practical applications.

The CDDT model was again applied to Steven and Haynes B_s data [5], the conditions for bainite being that:

(a) Growth must be diffusionless.
(b) Carbon may partition during nucleation.
(c) The stored energy must be temperature dependent, of the form given in reference [4].

The results are presented in figure 9 which reveals serious discrepencies, the calculations on average underestimating the B_s temperatures by some 100°C. The scatter is in fact far greater than would be expected from reference [4] where the B_s temperature was fully accurately estimated for Fe–C alloys. The reasons for these discrepencies are not clear but it is useful that there is a general trend as function of alloy content. The variation in stored energy with the experimental B_s temperatures of Steven and Haynes data [5] is shown in figure 10.

4. Conclusions

The CDDT model is able to accurately predict the martensite-start temperature of alloyed steels, the level of accuracy matching any previous empirical analysis. On the other hand, significant difficulties remain as far as the bainite-start temperatures are concerned, the reasons for which are not clear. The calculations consistently underestimate the experimental data. The trend in B_s temperatures nevertheless appears to be roughly predicted.

Acknowledgments

S Mujahid would like to express his gratitude to the Government of Pakistan and the Pakistan Atomic Energy Commission for financial support.

References

[1] Olson G B, Bhadeshia H K D H and Cohen M 1989 *Acta Metall.* **37** 381
[2] Olson G B, Bhadeshia H K D H and Cohen M 1990 *Metall. Trans.* A **21** 805
[3] Bhadeshia H K D H and Christian J W 1990 *Metall. Trans.* A **21** 767
[4] Mujahid S A and Bhadeshia H K D H 1993 *Acta Metall.* **41** 767
[5] Steven W and Haynes A G 1956 *Journal of the Iron and Steel Institute* **183** 449
[6] Ivantsov P G 1947 *Dokl. Akad. Nauk. SSSR* **58** 567
[7] Trivedi R and Pound G M 1967 *J. Appl. Phys.* **38** 3569
[8] Siller R H and McLellan R B 1970 *Metall. Trans.* **1** 985
[9] Bhadeshia H K D H 1981 *Met. Sci.* **15** 477
[10] Grujicic M, Olson G B and Owen W S 1985 *Metall. Trans.* A **16** 1713
[11] Grujicic M, Olson G B and Owen W S 1985 *Metall. Trans.* A **16** 1723
[12] Grujicic M, Olson G B and Owen W S 1985 *Metall. Trans.* A **16** 1735
[13] Olson G B unpublished research (referenced in Olson G B, Bhadeshia H K D H and Cohen M 1989 *Acta Metall.* **37** 381)
[14] Nabarro F R N 1982 *Proc. Royal Soc.* A **381** 285
[15] Christian J W 1965 Physical Properties of Martensite and Bainite *Iron and Steel Institute Special Report* **93** (London: Iron and Steel Institute)
[16] Baker J C and Cahn J W 1969 *Acta Metall.* **17** 575
[17] Aziz M J 1982 *J. Appl. Phys.* **53** 1158
[18] Aziz M J 1983 *Appl. Phys. Lett.* **43** 552

[19] Bhadeshia H K D H 2001 *Bainite in Steels* 2nd Edn (London: The Institute of Materials) pp 152–155
[20] World wide web: www.msm.cam.ac.uk/map/mcpmain.html
[21] Bhadeshia H K D H and Edmonds D V 1980 *Acta Metallurgica* **28** 1265
[22] Kaufman L and Cohen M 1956 *J. Metals* 1393
[23] Kaufman L and Cohen M 1958 *Progress in Metal Phys.* **7** 165
[24] Bhadeshia H K D H 1981 *Metal Science* **15** 175
[25] Lacher J R 1937 *Proc Cambridge Phil Soc* **33** 518
[26] Fowler R H and Guggenhiem 1939 *Statistical Thermodynamics* and *Proceeding* (New York: Cambridge Univ Press) p 442
[27] Bhadeshia H K D H 1981 *Metal Science* **15** 178
[28] Bhadeshia H K D H 1981 *Acta Metallurgica* **29** 1117